Applied and Environmental Microbiology, June 2007, p. 3859–3864 Vol. 73, No. 12
0099-2240/07/$08.00+0 doi:10.1128/AEM.02986-06

Flux Analysis of Central Metabolic Pathways in *Geobacter metallireducens* during Reduction of Soluble Fe(III)-Nitrilotriacetic Acid▽§

Yinjie J. Tang,[1,2,7]† Romy Chakraborty,[3,7]† Héctor García Martín,[4] Jeannie Chu,[1,2] Terry C. Hazen,[3,7] and Jay D. Keasling[1,2,5,6,7]*

Synthetic Biology Department, Physical Biosciences Division, Lawrence Berkeley National Laboratory, Berkeley, California 94720[1]; Department of Chemical Engineering, University of California at Berkeley, Berkeley, California 94720[2]; Center for Environmental Biotechnology, Lawrence Berkeley National Laboratory, Berkeley, California 94720[3]; DOE Joint Genome Institute, 2800 Mitchell Drive, Walnut Creek, California 94598[4]; Department of Bioengineering, University of California at Berkeley, Berkeley, California 94720[5]; California Institute for Quantitative Biomedical Research (QB3), University of California at Berkeley, Berkeley, California 94720[6]; and Virtual Institute for Microbial Stress and Survival[7]‡

Received 22 December 2006/Accepted 18 April 2007

We analyzed the carbon fluxes in the central metabolism of *Geobacter metallireducens* strain GS-15 using ^{13}C isotopomer modeling. Acetate labeled in the first or second position was the sole carbon source, and Fe-nitrilotriacetic acid was the sole terminal electron acceptor. The measured labeled acetate uptake rate was 21 mmol/g (dry weight)/h in the exponential growth phase. The resulting isotope labeling pattern of amino acids allowed an accurate determination of the in vivo global metabolic reaction rates (fluxes) through the central metabolic pathways using a computational isotopomer model. The tracer experiments showed that *G. metallireducens* contained complete biosynthesis pathways for essential metabolism, and this strain might also have an unusual isoleucine biosynthesis route (using acetyl coenzyme A and pyruvate as the precursors). The model indicated that over 90% of the acetate was completely oxidized to CO_2 via a complete tricarboxylic acid cycle while reducing iron. Pyruvate carboxylase and phosphoenolpyruvate (PEP) carboxykinase were present under these conditions, but enzymes in the glyoxylate shunt and malic enzyme were absent. Gluconeogenesis and the pentose phosphate pathway were mainly employed for biosynthesis and accounted for less than 3% of total carbon consumption. The model also indicated surprisingly high reversibility in the reaction between oxoglutarate and succinate. This step operates close to the thermodynamic equilibrium, possibly because succinate is synthesized via a transferase reaction, and the conversion of oxoglutarate to succinate is a rate-limiting step for carbon metabolism. These findings enable a better understanding of the relationship between genome annotation and extant metabolic pathways in *G. metallireducens*.

Geobacter species are known to be one of the dominant groups of microorganisms mediating iron reduction in the environment (21). They have been found to be ubiquitous in a myriad of subsurface environments. Detailed studies of their metabolism have revealed them to be capable of bioremediation of several heavy metals, including uranium, plutonium, technetium, and vanadium, as well as biodegradation of several organic contaminants, including monoaromatic hydrocarbons (16, 17, 26). More recently, *Geobacter* species have been used to generate electricity from waste organic matter (2, 15, 19). These unique metabolisms make *Geobacter* species important players in the contaminated subsurface environment (18). *Geobacter metallireducens* was the first iron-reducing organism isolated that coupled complete oxidation of organic acids with reduction of iron oxides (20, 21). It completely oxidizes organic carbons such as fatty acids, alcohols, and monoaromatic compounds via the tricarboxylic acid (TCA) cycle (3, 20) coupled with the reduction of iron. The genomes of several *Geobacter* species have been sequenced, and proteome data are also available (5, 24). While the genome sequence and proteome are important for understanding *Geobacter*, they are not necessarily accurate representations of cell physiology and metabolism.

To quantitatively analyze central metabolism in *Geobacter sulfurreducens*, a constraint-based model was developed using the annotated genome sequence and a series of physicochemical constraints (thermodynamic directionality, enzymatic capacity, and reaction stoichiometry) (22). While the model provided important insight into energy conservation, biosynthesis of building blocks (such as amino acids), and the relationship of the genotype to its phenotype, underdetermined models require one to assume an objective function (i.e., maximizing the specific growth rate) that may or may not be accurate and underdetermined models may have difficulty predicting fluxes through reversible reactions or reactions that may form futile cycles (7, 32, 39). Further, genes are often incorrectly annotated in sequenced genomes, and incorporation of these reactions into the model can affect the flux calculation. Even when genes are properly annotated, the presence of a gene does not indicate if it is being expressed.

* Corresponding author. Mailing address: Berkeley Center for Synthetic Biology, 717 Potter Street, Building 977, Mail code 3224, University of California, Berkeley, CA 94720-3224. Phone: (510) 495-2620. Fax: (510) 495-2630. E-mail: keasling@berkeley.edu.

† These authors made equal contributions to the study.

‡ http://vimss.lbl.gov.

§ Supplemental material for this article may be found at http://aem.asm.org/.

▽ Published ahead of print on 27 April 2007.

Here we report a different approach to the analysis of fluxes in the central metabolic pathways of *G. metallireducens* GS-15. The cells were fed [^{13}C]acetate, and the distribution of the ^{13}C in amino acids was measured. Interpreted in light of the genome annotation, a model based on the atom transitions between metabolites in biochemical reactions calculated the fluxes through the central metabolic pathway (12, 32, 33, 35). The model did not require energy balances for the calculation and resolved bidirectional or futile reactions. This study provided flux information complementary to the recent in silico model predictions and extended our understanding of anaerobic carbon metabolism in *Geobacter* species.

MATERIALS AND METHODS

Growth conditions. All media and solutions were prepared using strict anaerobic techniques. The standard *G. metallireducens* bicarbonate-buffered freshwater medium was used (21) with one exception: 1/10 the vitamin mix solution was used to minimize the isotopomer measurement "noise" introduced by unlabeled carbon from vitamins. Briefly, the medium was boiled under a N_2-CO_2 (80:20, vol/vol) headspace in order to remove the dissolved oxygen. It was then dispensed into anaerobic pressure tubes or serum bottles under a N_2-CO_2 (80:20, vol/vol) headspace. The anaerobic pressure tubes or serum bottles were capped with thick butyl-rubber stoppers and sterilized. [1-^{13}C]sodium acetate and [2-^{13}C]sodium acetate (both of 99% purity) were obtained from Cambridge Isotope Laboratories Inc. (Andover, MA). Anoxic aqueous stock solutions of ferric nitrilotriacetic acid (NTA) (1 M), [1-^{13}C]sodium acetate (1 M), or [2-^{13}C]sodium acetate (1 M) were prepared under a headspace of N_2-CO_2. These stocks were delivered anaerobically into culture tubes and serum bottles via a needle. *G. metallireducens* GS-15 was routinely cultured on anaerobic basal medium (21) using 5 mM acetate and 15 mM Fe-NTA as the electron donor and acceptor, respectively, under a N_2-CO_2 (80:20, vol/vol) headspace. A 10% inoculum from the unlabeled stock culture was made in the [1-^{13}C]acetate or [2-^{13}C]acetate medium containing equivalent amounts of electron donor and acceptor. After growth reached the mid-log phase, cells were transferred again into the same labeled medium to minimize the effect of unlabeled carbon from the initial inoculum. This subculture protocol was repeated twice. All incubations were performed at 30°C.

Determining metabolite concentrations and biomass composition. The standard ferrozine assay was used to measure Fe(II) concentration during growth on acetate and Fe-NTA (21). Cell counts were performed using a microscope and acridine orange to stain cells. Briefly, a 100-μl sample was added to a 900-μl, 0.1% sodium polyphosphate solution and mixed well. This cell suspension (10 μl) was pipetted onto a 6-mm well of a slide. The slide was dried and heat fixed. Acridine orange stain (25 μl) was used to stain wells containing several dilutions of the cell samples. The slides were incubated in the dark for 2 min, washed, and then dried; the cells were counted using fluorescent microscopy. The concentrations of acetate in the culture supernatant (following centrifugation of the culture at 10,000 × *g* for 20 min at 4°C) were measured using enzyme assays (r-Biopharm, Darmstadt, Germany). The amino acid composition of the biomass protein was quantified using a Beckman 6300 amino acid analyzer (Beckman Coulter), performed by the Molecular Structure Facility at the University of California, Davis (http://msf.ucdavis.edu). Biomass constituents were taken from the literature (22): protein, 46%; RNA, 10%; DNA, 4%; lipids, 15%; total carbohydrate, 15%; lipopolysaccharides, 4%; and peptidoglycan, 4%. Those data were the initial estimates for the isotopomer model to calculate fluxes into biomass.

Isotopomer analysis of protein amino acids by GC-MS (33–35). A 200-ml cell culture (2×10^8 cells/ml) was harvested by centrifugation at 10,000 × *g* for 20 min at 4°C and sonicated subsequently for 3 min. The protein from the resulting lysate was precipitated using trichloroacetic acid and then hydrolyzed in 6 M HCl at 100°C for 24 h. The amino acid-HCl solution was dried under nitrogen flow overnight. Gas chromatography-mass spectrometry (GC-MS) samples were prepared in 100 μl tetrahydrofuran (THF) and 100 μl *N*-(tert-butyldimethylsilyl)-*N*-methyl-trifluoroacetamide (Sigma-Aldrich). These samples were derivatized at 70°C for 1 h, producing tert-butyldimethylsilyl derivatives (33–35). One microliter of the derivatized sample was injected into a gas chromatograph (model HP6890; Agilent) equipped with a DB5-MS column (J&W Scientific, Falsom, CA) and analyzed using a mass spectrometer (model 5973; Agilent). The GC column was held at 150°C for 2 min, heated at 3°C per minute to 280°C, heated at 20°C per minute to 300°C, and held for 5 min at that temperature.

Annotated pathway map and algorithm for flux calculation. The central biochemical pathways in *G. metallireducens* GS-15 include gluconeogenesis, the TCA cycle, and the pentose phosphate pathway (PPP) (1). Each reaction and its corresponding gene are listed in Table S1 in the supplemental material. To reduce computational time, the fluxes through the pools of amino acids, carbohydrate, and RNA/DNA were loosely constrained by the biomass production and the measured average biomass composition (see Table S2 in the supplemental material), and those fluxes were optimized using the isotopomer model based on the amino acid label information. The reversible reactions were characterized by their net flux, v_i, and their exchange flux, v_i^{exch}. The net flux was defined as the difference between forward and backward fluxes, $v_i^{\rightarrow} - v_i^{\leftarrow}$. The exchange flux was the smaller of the forward and backward fluxes, $\min(v_i^{\rightarrow}, v_i^{\leftarrow})$, and was used to calculate the exchange coefficient, exch_i, according to references 33 and 38:

$$v_i^{\text{exch}} = \frac{\text{exch}_i}{1 - \text{exch}_i} \quad (1)$$

Exchange coefficients for all reactions were searched in the range [0 1] (41). Since atom transitions between metabolites in the biochemical network were known and the path that each atom took through the network could be traced using the model, the steady-state isotopomer distributions in the intracellular metabolite pools for a given flux distribution were obtained via the isotopomer mapping matrices (29, 32) (using MATLAB 6.0; Mathworks); these isotopomer distributions were used to simulate MS data (m/z = M0, M1, M2. . .). Our isotopomer model, like most nonlinear systems, did not possess a simple analytic solution. The final solution in our isotopomer model was searched based on an objective function defined as

$$\varepsilon(v_n) = \sum_{i=1}^{a} \left(\frac{M_i - N_i(v_n)}{\delta_i} \right)^2 \quad (2)$$

where v_n is the unknown fluxes to be optimized in the model program, M_i is the measured MS data when [1-^{13}C]acetate or [2-^{13}C]acetate was used as the carbon source, δ_i is the corresponding measurement errors, and N_i is the corresponding model-simulated MS data when a complete set of flux distribution (v_n) and exchange coefficients were given to the isotopomer model. The optimal fluxes were calculated to be such that ε was minimized using a simulated annealing approach with different initial conditions (27, 33). The initial annealing temperature was set to 50 and the final one to 0.01, with the temperature being decreased 100 times by a set fraction each time. In each run, approximately 10,000 to 100,000 moves were used, and the algorithm was restarted from the final position several times to check the reliability of the minimum. The examples of MATLAB programs for calculation of flux and exchange coefficients are available at http://vimss.lbl.gov/DvHFlux/AdvancedCodesWithAMM_IMM.rar. The solution produced isotopomer predictions consistent with measured data from both [1-^{13}C]acetate and [2-^{13}C]acetate experiments.

RESULTS AND DISCUSSION

***G. metallireducens* GS-15 growth kinetics in minimal medium.** GS-15 grew in minimal medium and completely oxidized acetate as the sole carbon and energy source by reducing Fe^{3+} to Fe^{2+} (Fig. 1). The doubling time was ~5 h with a late mid-log-phase density of $\sim 2.3 \times 10^8$ cells/ml, and the corresponding biomass concentration was 4.8 ± 0.3 mg/liter with a yield of 3.2 g (dry weight)/mol acetate. In the final sampling point, about 1.5 mM acetate was consumed and 11 mM Fe^{2+} was generated (equivalent to dissimilating 1.4 mM acetate). This result indicates that the *Geobacter* strain's biomass yield from oxidization of acetate is three times lower than the thermodynamic yield predictions (16.8 g [dry weight]/mol acetate) (36, 40). Under standard conditions (1 atm and 25°C, indicated by θ), Fe^{3+} ($\Delta G^{\theta} = -24.38$ kcal/eq) has a similar electron potential as oxygen ($\Delta G^{\theta} = -25.28$ kcal/eq) (23). However, the *Geobacter* Fe(III) reduction site is extracellular (not in the cytoplasm); under Fe^{3+}-NTA reduction, the electrons have to

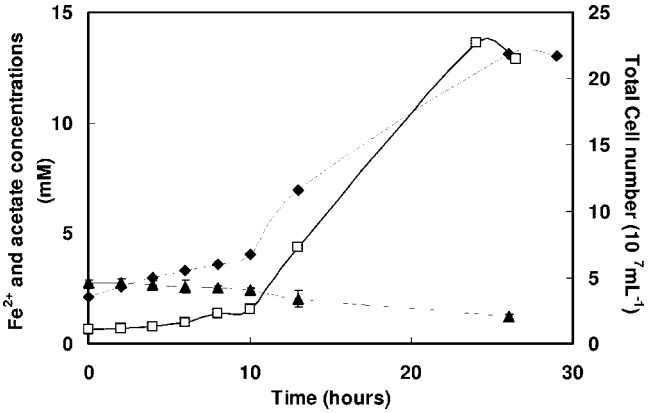

FIG. 1. *G. metallireducens* GS-15 growth kinetics in minimal medium. □, total cell number; ◆, Fe^{2+} concentration; ▲, acetate concentration.

be transported outside the cell or into the periplasmic cytochrome pool, but the protons remain in the cytoplasm (22). This could result in dissipation of the membrane potential and acidifying the cytoplasm, which in turn could reduce the biomass yield that results from acetate via Fe^{3+} reduction compared to that obtained during oxygen or fumarate reduction (9, 22).

Isotopomer analysis of labeling pattern in protein amino acids by GC-MS. Labeled acetate (first position or second position) was used in independent experiments. GS-15 was harvested in the exponential growth phase from each batch culture (a quasi-steady state that the cells are in under a balanced growth condition) (10, 28, 31). Two types of positively charged amino acid species from the biomass protein were clearly observed by GC-MS: unfragmented amino acids ($[M57]^+$) and fragmented species ($[M159]^+$) that had lost the α-carboxyl group (4, 6, 14, 37). The natural abundance of heavy isotopes common in organic molecules as well as in the derivatization agents was corrected for by using published algorithms (37). The corrected GC-MS data for eight key amino acids useful for model calculation, including $[M57]^+$ and $[M159]^+$, are provided in Table 1. The isotopomer distributions in the amino acids from hydrolyzed protein were used to examine the metabolic pathways. For example, the different labeling patterns of alanine and serine indicate that their precursors were not the same: alanine is derived from pyruvate,

TABLE 1. Measured fragment mass distributions for ^{13}C-labeled amino acids from *G. metallireducens* GS-15 hydrolysates[a]

Carbon source for culture	Amino acid (precursor)	Fragment	M_0	M_1	M_2	M_3
[1-^{13}C]acetate	Glycine (PGA)[b]	$[M57]^+$	0.15 ± 0.02	0.85 ± 0.03		
		$[M85]^+$	0.26 ± 0.02	0.74 ± 0.03		
	Serine (PGA)	$[M57]^+$	0.14 ± 0.02	0.83 ± 0.03	0.03 ± 0	
		$[M159]^+$	0.25 ± 0.02	0.75 ± 0.03	0.0 ± 0	
	Alanine (pyruvate)	$[M57]^+$	0.05 ± 0.02	0.94 ± 0.02	0.01 ± 0	
		$[M159]^+$	0.05 ± 0.02	0.95 ± 0.01	0 ± 0	
	Leucine (pyruvate + acetyl-CoA)	$[M159]^+$	0.01 ± 0	0.09 ± 0.02	0.87 ± 0.02	0.02 ± 0
	Isoleucine (OAA + pyruvate)	$[M159]^+$	0.01 ± 0	0.09 ± 0.01	0.88 ± 0.02	0.01 ± 0.01
	Glutamate (OXO)	$[M57]^+$	0.02 ± 0	0.77 ± 0.03	0.14 ± 0.02	0.03 ± 0.01
		$[M159]^+$	0.02 ± 0.01	0.83 ± 0.02	0.12 ± 0.02	0.02 ± 0.01
	Aspartate (OAA)	$[M57]^+$	0.04 ± 0.02	0.85 ± 0.03	0.10 ± 0.02	0.01 ± 0
		$[M159]^+$	0.42 ± 0.03	0.53 ± 0.03	0.03 ± 0.01	0.02 ± 0.01
	Histidine (C5P)	$[M57]^+$	0.04 ± 0.01	0.36 ± 0.02	0.55 ± 0.02	0.02 ± 0
		$[M159]^+$	0.06 ± 0.02	0.36 ± 0.02	0.53 ± 0.02	0.02 ± 0
	Phenylalanine (PEP + E4P)	$[M57]^+$	0.01 ± 0	0.07 ± 0.01	0.29 ± 0.04	0.49 ± 0.05
		$[M159]^+$	0.01 ± 0	0.07 ± 0.01	0.31 ± 0.04	0.46 ± 0.05
	Predicted $^{13}CO_2$		0.01			
	Predicted $^{13}C_1$ pool		0.02			
[2-^{13}C]acetate	Glycine (PEP)[b]	$[M57]^+$	0.75 ± 0.03	0.15 ± 0.02	0.10 ± 0.02	
		$[M85]^+$	0.79 ± 0.03	0.21 ± 0.02		
	Serine (PEP)	$[M57]^+$	0.04 ± 0.01	0.70 ± 0.03	0.16 ± 0.02	
		$[M159]^+$	0.05 ± 0.02	0.79 ± 0.03	0.16 ± 0.02	
	Alanine (pyruvate)	$[M57]^+$	0.03 ± 0.01	0.93 ± 0.01	0.02 ± 0.01	
		$[M159]^+$	0.03 ± 0	0.93 ± 0.01	0.04 ± 0.01	
	Leucine (pyruvate + acetyl-CoA)	$[M159]^+$	0.01 ± 0	0.01 ± 0	0.04 ± 0.01	0.89 ± 0.02
	Isoleucine (OAA + pyruvate)	$[M159]^+$	0.01 ± 0	0.01 ± 0.01	0.05 ± 0.01	0.87 ± 0.01
	Glutamate (OXO)	$[M57]^+$	0.02 ± 0	0.01 ± 0	0.16 ± 0.01	0.74 ± 0.02
		$[M159]^+$	0.02 ± 0	0.02 ± 0	0.18 ± 0.02	0.78 ± 0.03
	Aspartate (OAA)	$[M57]^+$	0.02 ± 0.01	0.08 ± 0.01	0.18 ± 0.02	0.72 ± 0.03
		$[M159]^+$	0.03 ± 0.02	0.15 ± 0.02	0.48 ± 0.02	0.33 ± 0.02
	Histidine (C5P)	$[M57]^+$	0.02 ± 0	0.01 ± 0	0.15 ± 0.02	0.52 ± 0.03
		$[M159]^+$	0.03 ± 0.01	0.12 ± 0.01	0.49 ± 0.02	0.23 ± 0.02
	Phenylalanine (PEP + E4P)	$[M57]^+$	0.01 ± 0	0 ± 0	0.02 ± 0	0.38 ± 0.03
		$[M159]^+$	0.01 ± 0	0 ± 0	0.02 ± 0	0.36 ± 0.02
	Predicted $^{13}CO_2$		0.03			
	Predicted $^{13}C_1$ pool		0.82			

[a] ^{13}C-labeled biomass was sampled in the middle log phase. The standard deviations for GC-MS measurement were based on the triplicate experiments ($n = 3$). C5P, ribose-5-phosphate (or ribulose-5-phosphate or xylulose-5-phosphate); E4P, erythrose-4-phosphate; OAA, oxaloacetate; OXO, 2-oxoglutarate; PGA, 3-phosphoglycerate.
[b] Glycine fragmentation ($[M159]^+$) was not observed. $[M85]^+$ (loss of carboxyl group) was used instead.

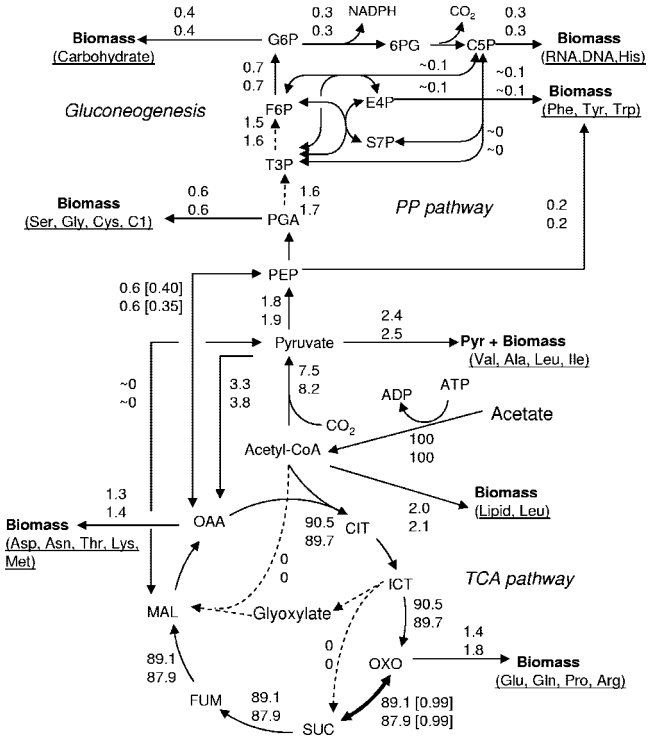

FIG. 2. Metabolic flux distribution in *G. metallireducens* GS-15 under Fe^{3+} reduction conditions. Flux was determined based on [1-^{13}C]acetate (upper numbers) and [2-^{13}C]acetate (lower numbers) experiments. The acetate uptake rate was 21 mmol/g (dry weight)/h. The data in brackets are the exchange coefficients. The dotted arrows indicate the absence of an annotated gene for the step. Abbreviations: 6PG, 6-phosphogluconate; ACoA, acetyl-CoA; C1, 5,10-methyl-THF; C5P, ribose-5-phosphate (or ribulose-5-phosphate or xylulose-5-phosphate); CIT, citrate; E4P, erythrose-4-phosphate; F6P, fructose-6-phosphate; G6P, glucose-6-phosphate; ICT, isocitrate; MAL, malate; OAA, oxaloacetate; OXO, 2-oxoglutarate; PGA, 3-phosphoglycerate; PYR, pyruvate. S7P, sedoheptulose-7-phosphate; SUC, succinate; T3P, triose-3-phosphate.

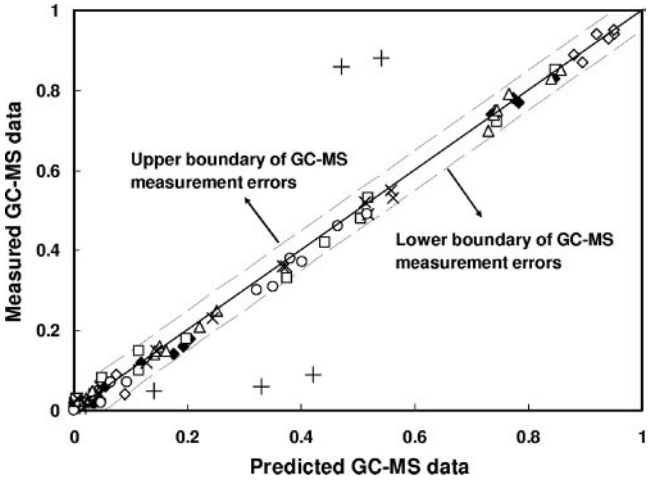

FIG. 3. Model quality test. ◆, glutamate data; □, aspartic acid data; ◇, alanine and leucine data; △, serine and glycine data; ×, histidine data; ○, phenylalanine data; +, isoleucine data (isoleucine data were not used as constraints for the model calculation). The absolute GC-MS measurement errors were based on the information in Table 1.

while serine is derived from phosphoglyceric acid. In each type of experiment, isotopomer patterns in some amino acids from the same precursor were similar and provided redundant isotopomer information (11): i.e., threonine and aspartate from oxaloacetate, and tyrosine and phenylalanine from PEP and erythrose-4-phosphate. Therefore, only one amino acid from each precursor listed in the table was used for model calculations. GC-MS cannot accurately measure the ion fragment $[M57]^+$ (no loss, $m/z = 302$) for leucine and isoleucine because of the overlay of mass peaks (the mass fragment with only the α and β carbons of leucine/isoleucine also has an m/z of 302) (37).

Determination of the flux distribution using the isotopomer model. The published annotated genome sequence of *G. metallireducens* indicates that several amino acid biosynthesis pathways (e.g., lysine and alanine) are incomplete (1). However, *G. metallireducens* is able to grow in minimal medium with acetate as its sole carbon source, and therefore it must contain complete energy and biosynthesis pathways for essential metabolites, i.e., *G. metallireducens* may have undocumented genes encoding some amino acid biosynthesis enzymes. The ^{13}C flux analysis can aid annotation of unannotated pathways. The isotopomer model calculation from two tracer experiments (with [1-^{13}C]acetate and [2-^{13}C]acetate) gave similar flux distribution results (Fig. 2). The predicted labeling patterns of all metabolites (except isoleucine), based on calculated fluxes and exchange coefficients, matched the measured data relatively well (deviations are within the noise from triplicate tracer experiments), and this indicates that model calculations are of good quality (Fig. 3). The discrepancy between the measured isoleucine $[M159]^+$ data and the model predictions indicates that isoleucine is not synthesized from oxaloacetate and pyruvate (Table 1) and an alternative isoleucine biosynthesis pathway may be present (see Fig. S1 in the supplemental material). The isotopomer labeling of isoleucine was identical to that of leucine from both tracer experiments, and this indicates that isoleucine has the same precursors (i.e., pyruvate and acetyl coenzyme A [acetyl-CoA]) as leucine. This hypothesis is supported by the recent discovery of citramalate synthase in *G. sulfurreducens*; thus, isoleucine is likely derived from acetyl-CoA and pyruvate via citramalate as an intermediate in *Geobacter* species (8; M. Coppi [University of Massachusetts, Amherst] and S. Van Dien [Genomatica, San Diego, CA], personal communication).

The conversion of acetate to acetyl-CoA (acetate uptake rate of 21 ± 1.6 mmol/g [dry weight]/h, assumed to be 100 in the model calculation) may be catalyzed by two independent enzymes (acetyl-CoA transferase or acetate kinase) (Fig. 2). The acetyl-CoA produced branched into three pathways: the major flow (19 mmol/g [dry weight]/h, relative flux [v] ≈ 90) was into a complete TCA cycle; the second flow was (1.7 mmol/g [dry weight]/h, $v \approx 8$) to pyruvate via pyruvate-ferredoxin oxidoreductase; and the third flow was into biomass production (e.g., synthesis of leucine and fatty acids). The genome annotation indicated that some key enzymes in gluconeogenesis were missing (EC 4.1.2.13, fructose-bisphosphate aldolase; EC 5.4.2.4, bisphosphoglycerate synthase; i.e., no re-

actions for glyceraldehyde-3-phosphate → β-D-fructose-1,6-bisphosphate). However, the tracer experiments indicated that gluconeogenesis is actually complete, and the total flux was 0.5 mmol/g (dry weight)/h ($v \approx 2.5$). The PPP is used for biosynthesis mainly when acetate is used as the sole carbon source. Although there are several alternative pathways to make ribose-5-phosphate (i.e., precursors of histidine and nucleotides), the model indicates that the major carbon flow to PPP is via the oxidative branch glucose-6-phosphate →6-phosphogluconate → ribose-5-phosphate, which generates NADPH (Fig. 2). In general, the isotopomer model gave results consistent with the previous predictions from a constraints-based model for a closely related species, *G. sulfurreducens* (22). However, the presence of PEP carboxykinase was not predicted by the constraints-based model but was found using the isotopomer model.

Characterization of GS-15 metabolism under Fe^{3+} reduction conditions. Previous reports indicate that *Geobacter* possesses two acetyl-CoA production routes (via acetyl-CoA transferase or acetate kinase/phosphotransacetylase) to secure sufficient flux for growth, whereas other acetate-degrading anaerobic bacteria often use one pathway for acetyl-CoA formation. This study also indicated the flexibility of central metabolism in other carbon utilization routes. For example, pyruvate carboxylase activity was present (0.7 mmol/g [dry weight]/h; $v \approx 3.6$); this is an alternative pathway to feed carbon into the TCA cycle by consuming ATP. Second, two carbon flows lead to PEP synthesis via pyruvate kinase/PEP synthase (~0.4 mmol/g [dry weight]/h; $v \approx 1.8$) or PEP carboxykinase (~0.1 mmol/g [dry weight]/h; $v \approx 0.6$). The presence of redundant pathways may stabilize cellular metabolism under conditions of environmental uncertainty (33). Meanwhile, the absence of the glyoxylate shunt (this pathway has not been annotated) was confirmed by the isotopomer analysis. On the other hand, the $NADP^+$-dependent malic enzyme, which is inhibited by the presence of acetyl-CoA (13) and whose corresponding gene was annotated in the genome, had no flux. These results are consistent with the predictions from the genome-scale, constraints-based model (22). With respect to energy production, zero flux through the glyoxylate shunt and malic enzyme maximizes the total carbon flow through the oxidative TCA cycle and thus produces the most reducing power (NADH).

In general, decarboxylation reactions, such as the oxidative reactions in the PPP and the TCA cycle, are frequently irreversible (30). However, the model predicted extremely high reversibility (exch = 0.99) in the reaction that converts oxoglutarate to succinate compared to those in other microorganisms (41). This reaction contains two steps and is usually catalyzed by the enzymes oxoglutarate oxidoreductase (oxoglutarate → succinyl-CoA; $\Delta G^0 = -33.5$ kJ/mol) and succinyl-CoA synthetase (succinyl-CoA → succinate; $\Delta G^0 = -2.9$ kJ/mol) (25). The free energy of both steps indicates a positive driving force for converting oxoglutarate to succinate. However, the succinyl-CoA synthetase activity is absent in *G. metallireducens*, and acetyl-CoA transferase instead is used to complete the reaction: succinyl-CoA (+ acetate) → succinate (+ acetyl-CoA) (13). The reason for the very high reversibility between oxoglutarate and succinate is likely that the accumulation of acetyl-CoA forces the reaction in the reverse direction and thus inhibits the rate of carbon metabolism through TCA cycle. This may explain the slow growth of *G. metallireducens* under iron-reducing conditions, even though the organism can use the complete TCA cycle to oxidize carbon substrates similarly to other aerobic bacteria.

Growth of *G. metallireducens* while oxidizing acetate requires incorporation of CO_2 into biomass (acetyl-CoA + CO_2 → pyruvate and pyruvate + CO_2 → oxaloacetate), and therefore our model evaluated the fate of the labeled ^{13}C of carbon dioxide. Experiments with [1-^{13}C]acetate and [2-^{13}C]acetate both indicated that the [^{13}C]CO_2 in the medium was below 3% of total CO_2 (Table 1). This is consistent with the fact that the labeled $^{13}CO_2$ produced from acetate oxidization is negligible compared to the $^{12}CO_2$ from the headspace gases (N_2-CO_2). The experiment performed with [1-^{13}C]acetate introduced very little ^{13}C (<3%) into the C_1 pool (5,10-methyl-THF), while most of the C1 pool was labeled (82%) in the [2-^{13}C]acetate experiments. This result confirms that C_1 metabolism is mainly via the serine pathway, i.e., serine is converted to glycine and a C_1 unit before being incorporated into protein. The carbon transition routes are $^*CH_3COOH \rightarrow {}^*CH_3COCOOH \rightarrow {}^*CH_2(OH)CH(NH_2)COOH \rightarrow CH_2NH_2COOH + {}^*C_1$ pool (where an asterisk indicates a labeled carbon).

In conclusion, this study demonstrates the usefulness of ^{13}C metabolic flux analysis as a tool for verifying genome annotation, characterizing the physiological state of microorganisms, and mapping the central metabolism in anaerobic bacteria. The results from our technique provide valuable information complementary to genome-based modeling approaches, resulting in a comprehensive understanding of central carbon metabolism in microorganisms. Our study indicates that *G. metallireducens* strain GS-15 utilizes the complete TCA cycle to oxidize acetate to CO_2 while reducing soluble Fe(III)-NTA. A futile pathway (pyruvate → oxaloacetate → PEP) is also evident by isotopomer data. Although the annotated genome indicates the absence of a few key enzymes in gluconeogenesis and some amino acid synthesis pathways, our ^{13}C tracer experiments demonstrate that those pathways are actually complete and *G. metallireducens* may contain some undocumented metabolic routes; e.g., an unusual isoleucine biosynthesis pathway possibly via citramalate as the intermediate is suggested by isotopic data. In combination with physiological data on the environmentally relevant microbe *G. metallireducens*, this study helps our understanding of carbon assimilation in the survival of such organisms in the environment.

ACKNOWLEDGMENTS

We thank M. Coppi (Department of Microbiology, University of Massachusetts, Amherst) and S. Van Dien (Genomatica, San Diego, CA) for advice on *Geobacter* anaerobic pathways. We also thank Michelle Chang (Department of Chemical Engineering, University of California, Berkeley) for help with experiments.

This work is part of the Virtual Institute for Microbial Stress and Survival (http://VIMSS.lbl.gov), supported by the U.S. Department of Energy, Office of Science, Office of Biological and Environmental Research, Genomics: GTL Program through contract DE-AC02-05CH11231 between the Lawrence Berkeley National Laboratory and the U.S. Department of Energy.

REFERENCES

1. **Alm, E. J., K. H. Huang, M. N. Price, R. P. Koche, K. Keller, I. L. Dubchak, and A. P. Arkin.** 2005. The MicrobesOnline Web site for comparative genomics. Genome Res. **15:**1015–1022.

2. **Bond, D. R., D. E. Holmes, L. M. Tender, and D. R. Lovley.** 2002. Electrode-reducing microorganisms that harvest energy from marine sediments. Science **295:**483–485.
3. **Childers, S. E., S. Ciufo, and D. R. Lovley.** 2002. *Geobacter metallireducens* access insoluble Fe(III) oxide by chemotaxis. Nature **416:**767–769.
4. **Dauner, M., and U. Sauer.** 2000. GC-MS analysis of amino acids rapidly provides rich information for isotopomer balancing. Biotechnol. Prog. **16:** 642–649.
5. **Ding, Y. H., K. K. Hixson, C. S. Giometti, S. A., A. Esteve-Nunez, T. Khare, S. L. Tollaksen, W. Zhu, J. N. Adkins, M. S. Lipton, R. D. Smith, T. Mester, and D. R. Lovley.** 2006. The proteome of dissimilatory metal-reducing microorganism *Geobacter sulfurreducens* under various growth conditions. Biochim. Biophys. Acta **1764:**1198–1206.
6. **Dookeran, N. N., T. Yalcin, and A. G. Harrison.** 1996. Fragmentation reactions of protonated α-amino acids. J. Mass Spectrometry **31:**500–508.
7. **Edwards, J. S., and B. O. Palsson.** 2000. The *Escherichia coli* MG1655 *in silico* metabolic genotype: its definition, characteristics, and capabilities. Proc. Natl. Acad. Sci. USA **97:**5528–5533.
8. **Eikmanns, B., D. Linder, and R. K. Thauer.** 1983. Unusual pathway of isoleucine biosynthesis in *Methanobacterium thermoautotrophicum*. Arch. Microbiol. **136:**111–113.
9. **Esteve-Nunez, A., M. Rothermich, M. Sharma, and D. R. Lovley.** 2005. Growth of *Geobacter sulfurreducens* under nutrient-limiting conditions in continuous culture. Environ. Microbiol. **7:**641–648.
10. **Fischer, E., and U. Sauer.** 2005. Large-scale *in vivo* flux analysis shows rigidity and suboptimal performance of *Bacillus subtilis* metabolism. Nat. Genet. **37:**636–640.
11. **Fischer, E., and U. Sauer.** 2003. Metabolic flux profiling of *Escherichia coli* mutants in central carbon metabolism using GC-MS. Eur. J. Biochem. **270:** 880–891.
12. **Fuhrer, T., E. Fischer, and U. Sauer.** 2005. Experimental identification and quantification of glucose metabolism in seven bacterial species. J. Bacteriol. **187:**1581–1590.
13. **Galushko, A. S., and B. Schink.** 2000. Oxidation of acetate through reactions of the citric acid cycle by *Geobacter sulfurreducens* in pure culture and in syntrophic coculture. Arch. Microbiol. **174:**314–321.
14. **Harrison, A. G.** 2001. Ion chemistry of protonated glutamic acid derivatives. Int. J. Mass Spectrom. **210/211:**361–370.
15. **Holmes, D. E., D. R. Bond, R. A. O'Neil, C. E. Reimers, L. R. Tender, and D. R. Lovley.** 2004. Microbial communities associated with electrodes harvesting electricity from a variety of aquatic sediments. Microb. Ecol. **48:**178–190.
16. **Lloyd, J. R., J. Chesnes, S. Glasauer, D. J. Bunker, F. R. Livens, and D. R. Lovley.** 2002. Reduction of actinides and fission products by Fe(III)-reducing bacteria. Geomicrobiol. J. **19:**103–120.
17. **Lloyd, J. R., V. A. Sole, C. V. G. Van Praagh, and D. R. Lovley.** 2000. Direct and Fe(II)-mediated reduction of technetium by Fe(III)-reducing bacteria. Appl. Environ. Microbiol. **66:**3734–3749.
18. **Lovley, D. R.** 2003. Cleaning up with genomics: applying molecular biology to bioremediation. Nat. Rev. Microbiol. **1:**35–44.
19. **Lovley, D. R., and R. T. Anderson.** 2000. Influence of dissimilatory metal reduction on the fate of organic and metal contaminants in the subsurface. Hydrogeology J. **8:**77–88.
20. **Lovley, D. R., S. J. Giovannoni, D. C. White, J. E. Champine, E. J. Phillips, Y. A. Gorby, and S. Goodwin.** 1993. *Geobacter metallireducens* gen. nov. sp. nov., a microorganism capable of coupling the complete oxidation of organic compounds to the reduction of iron and other metals. Arch. Microbiol. **159:**336–344.
21. **Lovley, D. R., and E. J. P. Phillips.** 1988. Novel mode of microbial energy metabolism: organic carbon oxidation coupled to dissimilatory reduction of iron or manganese. Appl. Environ. Microbiol. **54:**1472–1480.
22. **Mahadevan, R., D. R. Bond, J. E. Butler, A. Esteve-Nunez, M. V. Coppi, B. O. Palsson, C. H. Schilling, and D. R. Lovley.** 2006. Characterization of metabolism in the Fe(III)-reducing organism *Geobacter sulfurreducens* by constraint-based modeling. Appl. Environ. Microbiol. **72:**1558–1568.
23. **McFarland, M. J., and R. C. Sims.** 1991. Thermodynamic framework for evaluating PAH degradation in the subsurface. Ground Water **29:**885–896.
24. **Methe, B. A., K. E. Nelson, J. A. Eisen, I. T. Paulsen, W. Nelson, J. F. Heidelberg, D. Wu, M. Wu, N. Ward, M. J. Beanan, R. J. Dodson, R. Madupu, L. M. Brinkac, S. C. Daugherty, R. T. DeBoy, A. S. Durkin, M. Gwinn, J. F. Kolonay, S. A. Sullivan, D. H. Haft, J. Selengut, T. M. Davidsen, N. Zafar, O. White, B. Tran, C. Romero, H. A. Forberger, J. Weidman, H. Khouri, T. V. Feldblyum, T. R. Utterback, S. E. Van Aken, D. R. Lovley, and C. M. Fraser.** 2003. Genome of *Geobacter sulfurreducens*: metal reduction in subsurface environments. Science **302:**1967–1969.
25. **Nelson, D. L., and M. M. Cox.** 2000. Lehninger principles of biochemistry. Worth Publishers, New York, NY.
26. **Ortiz-Bernad, I., R. T. Anderson, H. A. Vrionis, and D. R. Lovley.** 2004. Vanadium respiration by *Geobacter metallireducens*: novel strategy for in situ removal of vanadium from groundwater. Appl. Environ. Microbiol. **70:**3091–3095.
27. **Press, W. H., S. A. Teukolsky, W. T. Vetterling, and B. P. Flannery.** 1992. Numerical recipes in FORTRAN, 2nd ed. Cambridge University Press, Cambridge, United Kingdom.
28. **Sauer, U., D. R. Lasko, J. Fiaux, M. Hochuli, R. Glaser, T. Szyperski, K. Wuthrich, and J. E. Bailey.** 1999. Metabolic flux ratio analysis of genetic and environmental modulations of Escherichia coli central carbon metabolism. J. Bacteriol. **181:**6679–6688.
29. **Schmidt, K., M. Carlsen, J. Nielsen, and J. Villadsen.** 1997. Modeling isotopomer distributions in biochemical networks using isotopomer mapping matrices. Biotechnol. Bioeng. **55:**831–840.
30. **Schmidt, K., J. Nielsen, and J. Villadsen.** 1999. Quantitative analysis of metabolic fluxes in *Escherichia coli*, using two-dimensional NMR spectroscopy and complete isotopomer models. J. Biotechnol. **71:**175–190.
31. **Stelling, J., U. Sauer, Z. Szallasi, F. Doyle, and J. Doyle.** 2004. Robustness of cellular functions. Cell **118:**675–685.
32. **Stephanopoulos, G. N., A. A. Aristidou, and J. Nielsen.** 1998. Metabolic engineering principles and methodologies. Academic Press, San Diego, CA.
33. **Tang, Y. J., J. S. Hwang, D. Wemmer, and J. D. Keasling.** 2007. The *Shewanella oneidensis* MR-1 fluxome under various oxygen conditions. Appl. Environ. Microbiol. **73:**718–729.
34. **Tang, Y. J., A. L. Meadows, J. Kirby, and J. D. Keasling.** 2007. Anaerobic central metabolic pathways in *Shewanella oneidensis* MR-1 reinterpreted in the light of isotopic metabolite labeling. J. Bacteriol. **189:**894–901.
35. **Tang, Y. J., F. Pingitore, A. Mukhopadhyay, R. Phan, T. C. Hazen, and J. D. Keasling.** 2007. Pathway confirmation and flux analysis of central metabolic pathways in *Desulfovibrio vulgaris* Hildenborough using GC-MS and FT-ICR mass spectrometry. J. Bacteriol. **189:**940–949.
36. **VanBriesen, J. M.** 2002. Evaluation of methods to predict bacterial yield using thermodynamics. Biodegradation **13:**171–190.
37. **Wahl, S. A., M. Dauner, and W. Wiechert.** 2004. New tools for mass isotopomer data evaluation in ^{13}C flux analysis: mass isotope correction, data consistency checking, and precursor relationships. Biotechnol. Bioeng. **85:** 259–268.
38. **Wiechert, W., and A. A. de Graaf.** 1997. Bidirectional reaction steps in metabolic networks. I. Modeling and simulation of carbon isotope labeling experiments. Biotechnol. Bioeng. **55:**101–117.
39. **Wiechert, W., M. Mollney, S. Petersen, and A. A. de Graaf.** 2001. A universal framework for ^{13}C metabolic flux analysis. Metab. Eng. **3:**265–283.
40. **Xiao, J., and J. M. VanBriesen.** 2006. Expanded thermodynamic model for microbial true yield prediction. Biotechnol. Bioeng. **93:**110–121.
41. **Zhao, J., and K. Shimizu.** 2003. Metabolic flux analysis of *Escherichia coli* K12 grown on 13C-labeled acetate and glucose using GC-MS and powerful flux calculation method. J. Biotechnol. **101:**101–117.